ELSEVIER

High-frequency underway analysis of ammonium in coastal waters using an integrated syringe-pump-based environmental-water analyzer (*i*SEA)

Peicong Li, Yao Deng, Huilin Shu, Kunning Lin, Nengwang Chen, Yiong Jiang, Jixin Chen, Dongxing Yuan, Jian Ma*

State Key Laboratory of Marine Environmental Science, Fujian Provincial Key Laboratory for Coastal Ecology and Environmental Studies, College of the Environment and Ecology, Xiamen University, Xiamen 361102, People's Republic of China

A B S T R A C T

Accurate methods and related robust analytical instruments for sensitive shipboard determination of ammonium in coastal waters are highly desirable for both oceanographers and environmental scientists. In this study, a multipurpose *i*ntegrated syringe-pump-based environmental-water analyzer (*i*SEA) was combined with an on-line filtration system for underway analysis of ammonium in coastal areas. The chemistry is based on a modified indophenol method using o-phenylphenol. The effects of reagent concentrations and sample temperatures were evaluated. The detection limit was 0.15 μM with a 3-cm Z-flow cell, and the linearity was as high as 200 μM. The relative standard deviations at different concentrations (2, 10, and 20 μM) were 2.2%, 0.33%, 0.32% (n = 11). For n = 288 and without any stoppage during repeated analysis for 24 h, the relative standard deviation was 0.85%. The sample throughput was 12 h^{-1}. The effects of salinity and five organic nitrogen compounds were evaluated and showed no interference using the proposed protocol for ammonium analysis. Between results obtained by reference and the present methods, there were no significant differences in the measurements of reference materials and different aqueous samples (n = 51). The analyzers worked well in the transect of 420 km during 7 cruises. A total of 716 analyses were performed automatically on board, demonstrating the capability of *i*SEA in automated real-time mapping of ammonium distribution in a shipboard laboratory.

1. Introduction

The nitrogen cycle plays a key role in determining the ecological status of aquatic environments because nitrogen is one of the major limiting nutrients in marine waters [1,2]. The marine nitrogen cycle is much more complex than that of either phosphorus or silicon because of its wide range of redox states (−3 to +5). Ammonium is the most reduced form of inorganic nitrogen available and it is preferentially assimilated by some marine phytoplankton. Thus, it is the mostly rapidly cycled nitrogen compound in waters in nature [3]. The study of ammonium in marine environment is very important because it adversely affects on various aquatic organisms [2]. Higher concentration of ammonium, especially ammonia, can be toxic to aquatic organisms. Therefore, the concentration of ammonium is a significant indicator of water quality [4]. In many estuary and coastal areas, there is elevated input of ammonium from anthropogenic sources (e.g., industrial effluent and agricultural runoff) as well as from natural sources, and this can lead to eutrophication accompanied by harmful algal blooms, decreased oxygen levels, and death of biota [5,6]. Because of complex variations in tide, season, upwelling, surrounding landscape, anthropogenic inputs, or processes such as adsorption/desorption by particulates and sediments, uptake, and biological activity, ammonium exhibit a large concentration gradient from nanomolar to several micromolar in estuary and coastal waters [7–9]. Therefore, spatially and temporally detailed measurement of ammonium concentrations in estuary and coastal waters is essential for enhancing our understanding of nitrogen biogeochemical processes and for improving predictive models in freshwater-estuary-coastal-marine systems [4,5,7,9].

Many analytical methods have been proposed for determining ammonium in water, and several comprehensive reviews have been published regarding ammonium determination [7,10,11]. The three commonly used techniques for ammonium measurement are gas diffusion, *o*-phthaldialdehyde-based fluorometric detection, and the classic Berthelot reaction-based indophenol blue (IPB) method [7]. Many improved protocols or new methods can be found in the literature. Some examples of publications in 2018 include incorporating membraneless vaporization units and a flow-through contactless conductivity detector [12], a slab optical waveguide sensor-based on ionic liquid [13], an

Table 1
Summary of on-board analysis using flow analysis techniques for measuring ammonium since 2000.

Year	Technique	Chemistry	LOD (nM)	Concentration range (µM)	Throughput, h^{-1}	Matrix	Ref.
2000	rFIA	OPA method	1	Up to 2	30	Seawater	[29]
2005	SFA, LWCC	IPB method	0.005	Up to 1	30	Seawater	[30]
2006	SIA	OPA method	50	Up to 20	120	River and seawater	[31]
2008	FIA	OPA method	1	Up to 0.6	8	Coastal water	[32]
2009	MPFS	Gas diffusion	10	Up to 18	8	Coastal water	[33]
2011	FIA	OPA method	5	Up to 25	12	Seawater	[34]
2011	SIA, SPE	IPB method	3.5	Up to 0.5	3	Seawater	[35]
2011	SIA	Gas diffusion	5500	Up to 222	28	Estuarine, coastal and well waters	[28]
2012	FBA	OPA method	10	Up to 10	4	Coastal water	[36]
2013	SIA, SPE	OPA method	0.12	Up to 0.3	5	Seawater	[37]
2015	CFA, LWCC	IPB method with OPP	4	Up to 0.2	10	Seawater	[38]
2017	FIA	OPA method	11	Up to 4	18	Coastal water	[39]
2018	rFIA	IPB method with OPP	80	Up to 35	30	River, coastal and estuarine waters	[24]

Abbreviations: rFIA, reverse flow injection analysis; SFA, segmented flow analysis; LWCC, liquid-core waveguide capillary cell; SIA, sequential injection analysis; MPFS, multi-pump flow system; SPE, solid phase extraction, FBA, flow batch analysis; CFA, continues flow analysis.

amperometric electrochemical sensor [14], colorimetric detection using modified Berthelot's reaction on porous paper [15] or a personal computer camera [16], smartphone detection with surface plasmon resonance of Ag nanoparticles [17], a passive sampler based on gas diffusion [18], a fluorescent probe and transducer dependent on fluorophotometry [19,20], membraneless gas separation coupled with fluorimetric sequential injection analysis [21], fluorescence detection with flow injection analysis (FIA) [22], and spectrophotometry with FIA [23] or reverse FIA [24]. Of these methods, few have the ability to measure ammonium concentration in saline waters [24]. Moreover, field analysis with an automated analyzer is highly necessary and in demand to eliminate the risk of sample degradation or contamination during collection, handling, and storage and to improve the temporal and spatial resolution of datasets [25]. Some on board monitoring systems that depend on FIA have been proposed for underway mapping of nutrient concentrations (e.g., phosphate [8], total phosphorus [26], and nitrate [27]) in estuarine and coastal areas. Table 1 summarizes reports of on-board analysis using flow analysis techniques for ammonium detection since 2000. As shown in Table 1, except for the gas diffusion method with SIA [28], all upper limits were less than 35 µM. Most of the methods were suitable for nanomolar level ammonium analysis in open ocean seawater, rather than micromolar level in estuaries and offshore area [29–39]. Similar comparison can also be found in other references [7,10]. However, the fully automated underway analysis of ammonium is still a challenge, especially in complex aquatic ecosystems where samples have varied salinity (0–35) and high turbidity [7,39].

Recently, we developed a new analytical system, named the *i*SEA (*i*ntegrated syringe-pump-based environmental-water analyzer), and used it for on-line monitoring of ammonium for 2 weeks in freshwater [40]. In this work, the chemistry was also based on the modified IPB method with OPP [41,42] with a focus on optimization in both pure water and a seawater matrix. Coupled with a simple on-line filtration system, *i*SEA was successfully applied in 7 cruises for underway analysis of ammonium in the Jiulongjiang Estuary, Xiamen Bay, and Dongshan Bay.

2. Experimental

2.1. Reagents and standards

All of the chemicals used in this study were analytical grade, purchased from Sinopharm Chemical Reagent Co., China, and used without purification. Pure water (18.2 MΩ cm) was obtained using a Millipore Purification System and was used throughout the experiments. An aged surface oligotrophic seawater collected from the South China Sea, which has only nanomolar level ammonium [43], was used as low

nutrient seawater (LNSW) to study the matrix effects.

Alkaline OPP stoke solution (20 g/L) was prepared by dissolving 2 g of OPP and 1 g of NaOH in 100 mL of water. OPP working solution (2 g/L) was obtained by mixing 10 mL of OPP stock solution with 90 mL of ultrapure water. Alkaline sodium dichloroisocyanurate (NaDTT) stock solution (10 g/L) was prepared by dissolving 1 g of NaDTT (Sigma-Aldrich, USA) and 1 g of NaOH in 100 mL of water. NaDTT working solution (1 g/L) was obtained by mixing 10 mL of NaDTT stock solution with 90 mL of ultrapure water. Alkaline sodium nitroprusside (NP) solution (5 g/L) was prepared by dissolving 0.5 g of NP (Merck-Chemicals, Germany) and 0.3 g of NaOH in 100 mL of water. The reagent bottles were sealed in plastic bags to prevent atmospheric ammonia contamination. Ammonium stock solution was prepared by dissolving oven-dried (105 °C for 2 h) NH_4Cl (Fluka, USA) in pure water.

Five organic nitrogen compounds (glycine, urea, 4-aminoantipyrine, nicotinic acid, and L-glutamic) were used for interference studies. Glycine, urea, and 4-aminoantipyrine stock solutions were each prepared at a concentration of 100 mM. Nicotinic acid and L-glutamic stock solutions were each prepared at a concentration of 10 mM. All of the stock solutions were stored at 4 °C when not in use. Certified materials of ammonium (GSBZ50005-88, Batch No. 200575 and No. 2005100) were purchased from the Institute for Environmental Reference Materials, the Ministry of Environmental Protection, China.

Exposure of reagents and standards to ambient air was minimized to avoid NH_3 contamination from ambient air. Acidic traps (made of acid-washed silica) were used to protect reagent and standard solutions from atmospheric ammonia [43].

2.2. Description of the apparatus

A schematic diagram of the underway sampling module, on-line filtration module, and detection module is illustrated in Fig. 1-A. In the sampling module, a self-priming pump (FL-43, SURGEflo, China) was used to pump water from a depth approximately 1-m below the surface up into the Ferrybox system (4H-JENA, Germany) at 10 L/min, where the salinity, temperature, turbidity, and chlorophyll concentration of water samples were measured. From the Ferrybox system, unfiltered samples were pumped into a 100 mL plastic bottle using a peristaltic pump (Masterflex L/S, Cole-Parmer, USA). The filtering module included a BT100-1L 6-channel peristaltic pump (Baoding Longer Precision Pump, China), a 28-position selection valve (VICI, Valco Instruments, USA), and 28 reusable polypropylene syringe filters. Unfiltered samples were passed through the 0.45 µm cellulose acetate filter membrane into a 15 mL centrifuge tube. By switching the valve position, the valve can be used to direct the sample flow to different filters connected to the valve ports. Filtered samples were aspirated to the *i*SEA from the centrifuge tube. The *i*SEA is mainly composed of a mini-
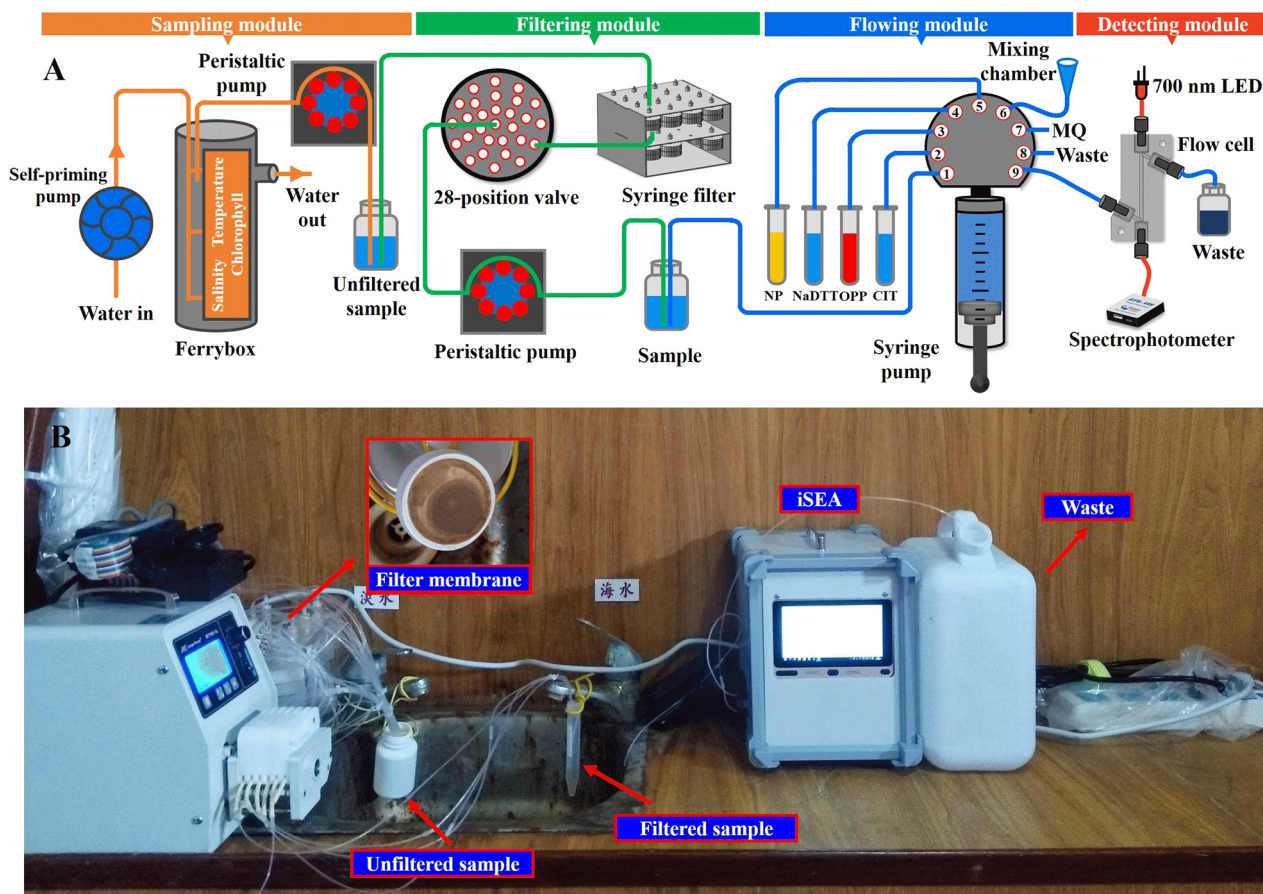
Fig. 1. Schematic illustration of *i*SEA for ammonium determination and underway sampling system (A). Photo of the on-line filtration system and *i*SEA during a cruise (B).

Table 2
Descriptions of analytical procedure for determining ammonium.

Step	Syringe pump	Valve position	Flow rate (mL/min)	Operation	Description
1–5	In	1	20	Aspirate 1000 μL of sample	Washing the mixing chamber and flow cell with sample, repeat 5 times.
	Out	6	60	Dispense 1000 μL of sample	
	In	6	60	Aspirate 1000 μL of sample	
	Out	8	60	Dispense 150 μL of sample	
	Out	9	60	Dispense 850 μL of sample	
6	In	1	20	Aspirate 500 μL of sample	Aspirate sample.
7–18	In	2/3/4/5	5	Aspirate the reagent	Aspirate 80 μL of citrate, 20 μL of OPP, 20 μL of NaDTT, 20 μL of NP sequentially,
	Out	6	60	Dispense the sample/ reagent mixture	mixing the sample and reagent for 3 cycles after each addition.
	In	6	60	Aspirate the sample/reagent mixture	
19–20	Out	8	60	Dispense 150 μL of mixture	Deliver the mixture to the flow cell.
	Out	9	60	Dispense 500 μL of mixture	

syringe pump (XCalibur, Tecan, USA) equipped with a 9-port distribution valve and a gas-tight 1.0 mL syringe (Hamilton, USA); by switching the valve position and moving the syringe plunger, different volumes of sample and reagents are delivered to the various components of the system. A conventional 1 mL pipette tip was used as a mixing chamber. Spectrophotometric detecting module consists of laboratory-made fiber optics and a 3-cm Z-flow cell, an STS mini-charge-coupled device (CCD) spectrophotometer (OceanOptics, USA) was used as the detector, and a 700 nm light-emitting diode (LED, EZDL-57C00, Shenzhen Yizhongda Co., China) driven at 20 mA was used as the light source. All of the pump and valve switching processes were operated with a software program written by LabVIEW 2016 (NI, USA).

Silicone tubing (Baoding Longer Precision Pump, China) was used as the pump tubing. The fluidic manifold was constructed using polytetrafluoroethylene tubing (0.75 mm i.d.) and standard 1/4–28 flangeless polyetheretherketone fittings (IDEX Health & Science LLC, USA).

2.3. Analytical procedure

The *i*SEA has previously been described in detail [40]. A mixing chamber is necessary in this situation because in saline waters, the sample/reagent mixture must be mixed completely after the addition of each reagent to reduce precipitation and to improve reproducibility. The syringe itself serves as the primary mixing chamber, and a 1 mL

pipette tip serves as the secondary a mixing chamber. It has been confirmed that this set up has better mixing conditions than typical mixing coil [44]. The bottom of the pipette tip was connected to port 6 of the selection valve. Liquid in the syringe was pushed into the pipette tip and then drawn back into the syringe. The sample/reagent mixture are thoroughly mixed after 3 mixing cycles.

The analytical procedure for the determining ammonium in coastal water is presented in Table 2. During steps 1–5, the syringe was connected to port 1, the syringe pump was used to aspirate 1000 μL of new sample into the syringe, and then the sample was transported through the mixing chamber (port 6) and flow cell (port 9). After cleaning five times, contamination from previous samples and carryover effects can be eliminated. During steps 6–18, 500 μL of sample were aspirated from port 1 into the syringe, and then 80 μL of citrate (port 2), 20 μL of OPP (port 3), 20 μL of NaDTT (port 4), and 20 μL of NP (port 5) were sequentially aspirated into the syringe. Three mixing cycles after the addition of each reagent were needed for sample/reagent mixing. During steps 19–20, the mixture was delivered to the flow cell (port 9) and stopped in the flow cell for 240 s, during which time the STS spectrophotometer continuously recorded the spectrum of the chemical reaction. To minimize the interference of bubbles, 150 μL of solution was pushed out as waste via port 7 before the sample or mixture was dispensed into the flow cell.

2.4. Sample collection and comparison of methods

Mineral water was purchased from the local market on the Xiang'an campus of Xiamen University. River water was collected from Min River and Jiulong River, Fujian, China. Seawater was collected from the surface of the South China Sea, Jiulongjiang Estuary and Xiamen Bay. Field calibration and comparison were performed using a collection of discrete samples that coincided with the time of sensor measurements. These samples were filtered through a 0.45 μm syringe-type polyether sulfone filter immediately after collection, and the filtered samples were stored at 4 °C and analyzed within 24 h.

The reference method for determining ammonium was a manual method based on the modified IPB method with OPP that was presented in our previous work [42]. A UV–Vis spectrophotometer (V1100D, Mapada Instruments, China) equipped with 1-cm and 5-cm path length cuvettes was used for absorbance measurements using the manual reference method.

2.5. Underway sampling of surface seawater

The lag time between when samples are pumped into the Ferrybox and when they reach the *i*SEA was approximately 1 min. Therefore, all of the data on the determination time of ammonium were adjusted by 1 min to ensure that the time data obtained from the *i*SEA and Ferrybox for the same sample were consistent.

A single filter membrane can be used for at least 5 h even when used in estuarine waters where the turbidity exceeded 100 NTU. When combined with a program-controlled 28-position selection valve, the filtration module can operate effectively for at least 5 days. As shown in Fig. 1-B, only one filter membrane was used during the whole Dongshan Swire Marine Station Cruise from May 27 to 29, 2018. The flow rate from the filter was typically between 8 and 10 mL/min. Filtered samples were delivered into a 15 mL centrifuge tube, which was also used as a primary de-bubbler. A similar semi-automated filtration system has been used by other groups in measuring particulate organic carbon in a coastal upwelling system [45].

3. Results and discussion

3.1. System design considerations

The system described here is designed for surface mapping

applications in coastal area and for on-line monitoring in a river or lake. The system needs to meet criteria of sensitivity, compactness, quick response, full automation, and robustness under harsh conditions.

In flow analysis techniques, air bubbles are one of the most complicated hindrances for long-term stable operation because they are almost unavoidable and lead to baseline drift and false signals. In some of our previous studies, cross-flow cells were developed to overcome the bubble problem, and these cells were shown to work well for field study [46,47]. However, the dead volume of the cell is relatively large for syringe pump-based analyzers. In flow techniques that use syringe pumps, such as the flow batch analysis, air bubbles are generally caused by the partial degassing of solutions at a pressure drop that occurs when solutions are aspirated [48]. To suppress the interference of air bubbles, the following measures were taken in this study: (1) Samples or reagents were aspirated at relatively low flow rates (≤ 2 mL/min) and liquids were dispensed at relatively high flow rates (≥ 3 mL/min) to decrease the generation of air bubbles, prevent the adsorption of bubbles onto hydrophobic surfaces of the tubing and flow cell, and eliminate bubbles that were stacked in the system. (2) A Z-flow cell with a small inner diameter (1.5 mm) of liquid path was selected so that the bubbles can be washed away at a high flow rate. (3) Generally, there were air bubbles floating on the liquid surface in the syringe, and 150 μL of solution was pushed out as waste before the sample or mixture was dispensed to the flow cell.

3.2. Optimization of reagent concentrations

A manual IPB method with OPP for ammonium determination in nature waters has been previously established [42]. Citrate was first added as the masking reagent to prevent the precipitation of insoluble hydroxides, then the reaction occurs with ammonium and hypochlorite provided by NaDTT to form a monochloramine, which next reacts with OPP under alkaline conditions in the presence of catalytic quantities of nitroprusside. Reagent concentrations play a key role in controlling the reaction kinetics of the Berthelot reaction, and the effects of different reagents on reaction kinetics have been previously evaluated in detail [42]. Under the optimized reagent concentrations, the modified method can be considered a salinity-interference-free method. However, the time for full reaction is different for samples with different salinities, and this results in a measurable salinity effect when the absorbance is determined under uncompleted reactions in *i*SEA. Therefore, the final concentrations of citrate and NP in the reaction mixture were chosen as 62.5 g/L and 0.16 g/L as were optimized in previous work [42]. The concentrations of OPP, NaDTT, and NaOH in NP solution were further optimized with an 8 μM standard solution prepared in pure water and LNSW to eliminate the salinity effect. Fig. 2 shows the effects of reagent concentrations on samples with salinity values of 0 (Fig. 2-A/C/E) and 35 (Fig. 2-B/D/F). The legends of Fig. 2-A/C/E reveal the absorbance difference in the final signal between samples in pure water and seawater matrix.

In seawater analysis, the buffering capacity of Mg–citrate systems can change the final pH and interfere with the color formation reaction. To compensate for this capacity, extra alkali reagent should be added to sea water samples for the optimal IPB color reaction [49]. Therefore, NaOH concentration in alkaline NP solution in the reaction mixture was evaluated over the range of 0–50 g/L. As seen in Fig. 2-A/B, in the lower range of tested NaOH concentrations (0–10 g/L), the reaction rate of sample prepared in seawater increased sharply with the increase of NaOH concentration, while for sample prepared in pure water, the effect of salinity on the reaction rate was slightly slower. For solutions both prepared in pure water and LNSW, all of the kinetics curves were almost identical when the NaOH concentration was higher than 10 g/L. Thus, the optimal NaOH concentration in NP solution was chosen to be 30 g/L.

The effects of OPP concentration were tested, and the results are shown in Fig. 2-C/D. The reaction was slower at high salinity (S = 35)
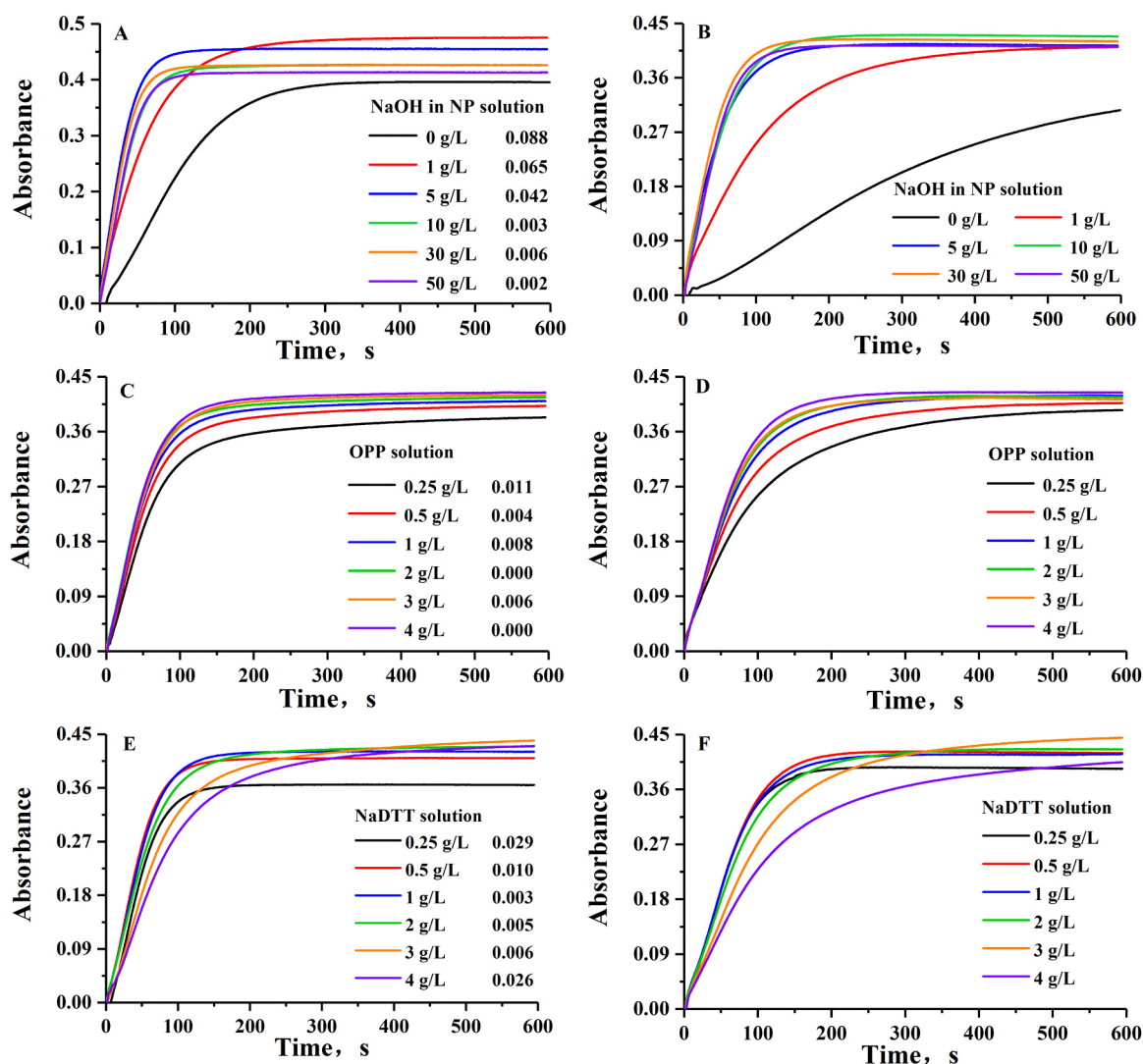
Fig. 2. Effects of reagent concentrations on reaction. A/B: Effects of NaOH concentration on kinetics with sample salinities of 0 (A) and 35 (B); C/D: Effects of OPP concentration on kinetics with sample salinities of 0 (C) and 35 (D); E/F: Effects of NaDTT concentration on kinetics with sample salinities of 0 (E) and 35 (F).
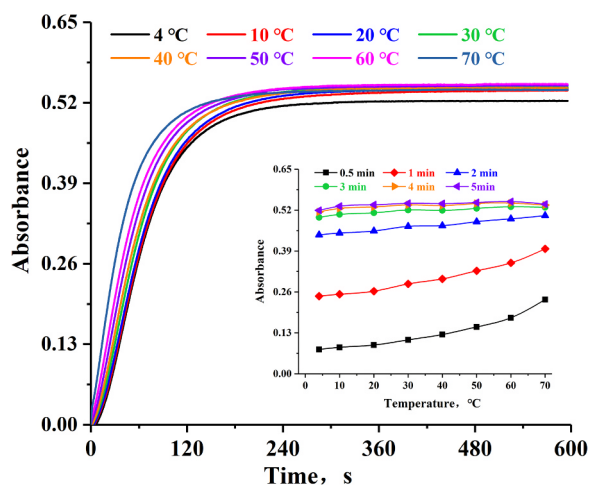

Fig. 3. Effects of sample temperature on reaction. Inset: Effects of sample temperature on signal at different sampling times.

than at low salinity (S = 0), and both reaction rate accelerated with an increase in OPP concentration (0.25–2 g/L). At higher OPP concentration (2–4 g/L), no differences were seen in either the kinetics curves or

the values of absolute deviation. Therefore, the optimal OPP stock solution concentration was chosen to be 2 g/L.

The effects of NaDTT concentration were studied, and the results are shown in Fig. 2-E/F. Lower NaDTT concentration resulted in a slower reaction rate of sample with salinity of 35 than for sample with salinity of 0. Absorbance increased and absolute deviation decreased with an increase in NaDTT concentration when the NaDTT stock solution concentration was between 0.25 and 1 g/L. The reaction rate decreased when the NaDTT concentration was higher (2–4 g/L). Therefore, the optimal NaDTT stock solution concentration was chosen to be 1 g/L of the stock solution.

3.3. Effects of sample temperature

The potential application of this analyzer is for field analysis on shipboard laboratories or on-line monitoring in remote areas, where the samples have various temperatures because of different sampling locations and seasons. Therefore, it is necessary to evaluate the effects of sample temperature on the reaction. To do so, the sample bottle was immersed in a water bath, and the temperature was changed from 4 to 70 °C. Under the tested temperatures, an increase in the sample temperature resulted in shorter color development time (Fig. 3). Because the sample temperature would increase or decrease to room
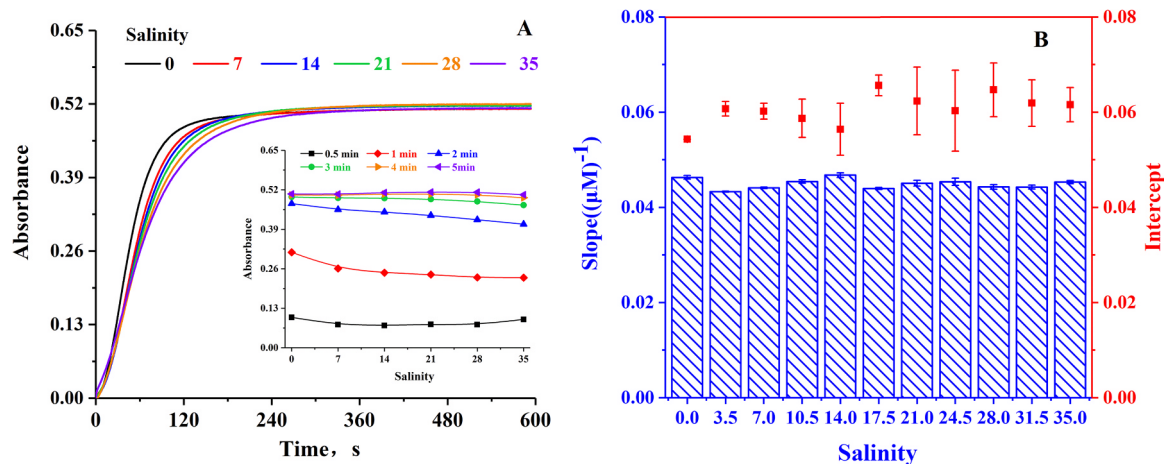
Fig. 4. Effects of sample salinity on reaction. A: Effects of sample salinity on reaction dynamics and signal at different sampling times. B: Slopes and intercepts of the standard curves at different salinities.

temperature when the sample and reagents were mixed, the effect of temperature on reaction time is significantly less than the effect reported in our previous study [42]. The inset of Fig. 3 shows how absorbance changes with reaction temperature with different reaction times. The relative standard deviation (RSD) of the response results was only 1.7% when the sample temperature was higher than 10 °C with a 5 min cycle time. Therefore, room temperature was selected to simplify the system and to avoid potential risks (e.g., bubble formation) that are encountered when using high temperature for the reaction.

3.4. Effects of sample salinity

The "pH-shift" phenomenon of the IPB method has been demonstrated in the work of Pai et al. [50], and this shift may affect the sensitivity of determining ammonium in coastal water. Therefore, it is necessary to study the effects of sample salinity on the results. Several seawater sample solutions with salinity values ranging from 0 to 35 were prepared using diluted aged seawater. As seen in Fig. 4-A, higher salinity yielded a faster reaction rate, and the inset of Fig. 4-A shows that the salinity effect can be ignored at the current analytical frequency (reaction for ~240 s and 5 min/sample). Fig. 4-B shows the slopes and intercepts of the calibration curves at different salinities, whose RSDs were 2.3% and 5.4%, respectively. Therefore, this method can be considered a salinity-interference-free method and can be used with various natural samples without calibration, which is significantly important for coastal water analysis.

3.5. Effects of organic nitrogen

There are various forms of organic nitrogen in natural waters, and these compounds can interfere with the determination of ammonium [51]. Nitrogen compounds selected for this study include urea, glycine, L-glutamic acid, nicotinic acid, and 4-aminoantipyrine. Urea is selected because it is a frequently occurring component; glycine and L-glutamic acid represent straight-chain amino acids; nicotinic acid and 4-aminoantipyrine represent cyclic amino acids [51]. The absorbance values of 10 μM ammonium solutions in the presence of 50 μM organic nitrogen compounds were tested using this method. Effects of organic nitrogen compounds were tested, and the results are tabulated in Table 3. Concentrations were calculated from absorbance according to the calibration curve. The percentage degradation of organic nitrogen compounds was defined as the ratio of the difference between the measured and spiked ammonium concentration (10 μM) to the actual ammonium value (10 μM). Concentrations were in the range of 9.36–12.1 μM, and the percentage degradation ranged from −1.28% to

Table 3
Effects of organic nitrogen compounds (50 μM) on measuring ammonium solution (10 μM).

Compound	Concentration, μM	Degradation percentage
Urea	9.36	−1.28%
Glycine	11.3	2.60%
L-glutamic	12.0	3.95%
Nicotinic acid	9.66	−0.69%
4-aminoantipyrine	12.1	4.23%

4.23%, which indicates that the effects of organic nitrogen compounds were negligible.

3.6. Analytical figures of merit

Under the optimized conditions, a series of ammonium standard solutions were prepared and analyzed using iSEA. The calibration curves were measured at 700 nm and 580 nm, which are the maximum absorption wavelength and the less sensitive detection wavelength, respectively. Calibration curves at two wavelengths are $A_{700\,nm}$ = (0.0459 ± 0.0002) *C (μM) + (0.048 ± 0.002) (R^2 = 0.9999, n = 7, range of 0–20 μM) and $A_{580\,nm}$ = (0.0066 ± 0.0001) *C (μM) + (0.019 ± 0.004) (R^2 = 0.9994, n = 7, range of 0–100 μM). Dilutions of the standard solutions were automated using same volume of pure water; the upper limit of the linear analytical range can be extended to 200 μM, and the regression equation is $A_{580\,nm}$ = (0.0034 ± 0.00004) *C (μM) + (0.016 ± 0.004) (R^2 = 0.9995, n = 7, range of 0–200 μM). Sample throughput with the optimized conditions was 12 h^{-1}. The typical signal output included the calibration curve, and the carryover effect is shown in Fig. 5.

The detection limit was calculated to be three times the standard deviation for measurements of the blank (n = 11) divided by the slope of the calibration curve, which was 0.15 μM. The RSDs for the repeated determination of samples (n = 11) at concentrations of 2, 10, and 20 μM were 2.2%, 0.33%, and 0.32%, respectively. Stability of response for 24 h is shown in the inset of Fig. 5; the RSD is 0.85% with an ammonium concentration of 10 μM (n = 288).

The carryover effect describes how analyte in a sample is "carried" by an analytical system "over" to the next sample, and this effect was quantified using the method proposed by Zhang [52]. The carry-over effect can be quantified using different equations. In this experiment, samples of low concentration (2.5 μM, i–2), high concentration (i–1, 10 μM) and low concentration (2.5 μM, i) were determined sequentially. The carry-over coefficient (K_{CO}) can be calculated as:
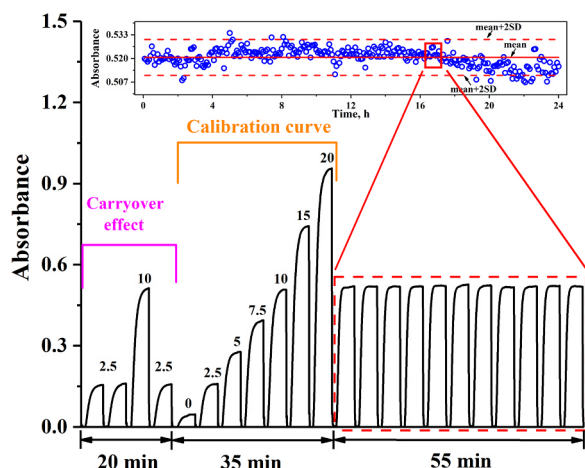
Fig. 5. Typical system signal output of carryover effect, calibration curve, and repeated analysis for 24 h.

$$K_{CO} = (A_i - A_{i-2})/A_{i-1}$$

where A_{i-2}, A_{i-1} and A_i are the measured absorbance values of samples i–2, i–1 and i, respectively.

The carryover coefficient for ammonium measurements was 0.0031. Thus, when going from a high concentration sample (10 µM) to a low concentration sample (2.5 µM), the carryover effect is negligible.

3.7. Reagent stability

Reagent stability is of great importance for long-term on-line ammonium monitoring in a river or on shipboard/underway seawater analysis. Thus, evaluating reagent stability is essential. As seen in Table 4, OPP, NaDTT, and NP solutions can be stable for at least 6 days when stored at 4 °C. After that, a decrease in reaction rate in saline samples was observed but not in freshwater samples. In long-term field application, a refrigerator is indispensable for storing reagents (e.g., a portable car refrigerator). Meanwhile, the OPP, NaDTT, and NP solutions should be freshly prepared if they have been stored for one week. The stored reagents can be used for a further 2 weeks, but the sensitivity of the saline samples drops to about 80% compared with that of the freshly prepared reagents (data not shown).

3.8. Method validation

The accuracy of the method was evaluated in three ways: measurement of certified materials, comparison with reference methods, and spiked recovery assay.

Diluted certified materials of ammonium (GSBZ50005-88, Batch No. 200575, and No. 2005100) with both pure water and LNSW (n = 18) were prepared as samples. Samples collected in Xiamen Bay and along the Jiulong River (n = 34) were analyzed using *i*SEA and a benchtop method. These samples exhibit a wide range of salinity and turbidity that are representative of typical samples from a river-estuary-coastal-marine system. The concentrations of ammonium obtained using the

Table 4
Stability study of reagents stored at 4 °C.

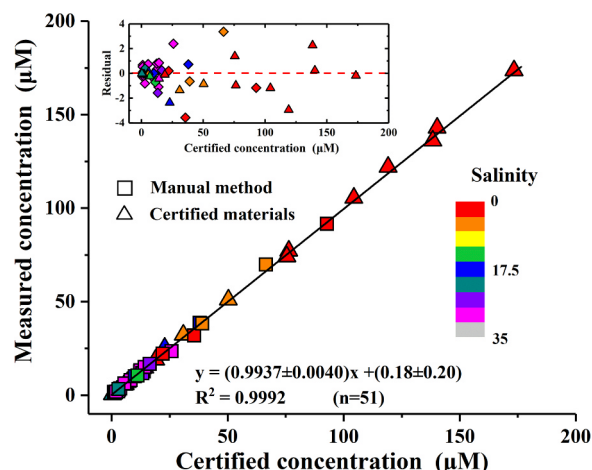| Time, day	Calibration curve	R²
1	y = (0.0448 ± 0.0003)*C (µM) + (0.049 ± 0.003)	0.9999
2	y = (0.0444 ± 0.0004) *C (µM) + (0.052 ± 0.005)	0.9998
3	y = (0.0443 ± 0.0008) *C (µM) + (0.057 ± 0.009)	0.9993
4	y = (0.0449 ± 0.0001) *C (µM) + (0.050 ± 0.002)	1.0000
5	y = (0.0438 ± 0.0007) *C (µM) + (0.048 ± 0.008)	0.9994
6	y = (0.0439 ± 0.0004) *C (µM) + (0.052 ± 0.005)	0.9998

Fig. 6. Comparison of analytical results obtained using *i*SEA and another method. Inset: Residual between the results obtained from the proposed method and those of the reference method at different ammonium concentrations.

analyzer were compared with the certified value and with the results obtained using the reference method. As seen in Fig. 6, the estimated slope and intercept do not differ significantly from the values of 1 and 0, respectively. The solid triangles or squares represent the salinity of the certified materials and samples, respectively. The samples covered a wide range of concentration (ranging from 0.38 µM to 177 µM) and salinity (ranging from 0 to 35). The inset of Fig. 6 shows that for the residuals, there is no significant difference between the results obtained using the proposed method and those obtained using the reference methods based on the paired Student's *t*-test at the 95% confidence level, which indicates excellent accuracy and minimal matrix effects.

To further assess the efficacy of the developed system, recovery studies were performed on water samples with different matrixes, including mineral water, river water, and seawater, and the results are presented in Table 5. Recoveries for the spiked samples varied from 94.3 ± 0.5% to 108 ± 1.0%, which indicates the applicability of the developed setup for determining ammonium in natural waters using various matrixes.

3.9. In-field application

The suitability of *i*SEA for underway mapping of ammonium in coastal waters has been tested in 7 cruises: Jiulongjiang Estuary-Xiamen Bay Sharing Cruise (4 cruises, April 23, April 24, July 23, and July 24, 2018) and Dongshan Swire Marine Station Sharing Cruise (3 cruises, May 27–29, 2018). The Jiulong River in southeast China has a drainage area of 14,740 km², and it is the second largest river in Fujian Province. The Jiulongjiang Estuary is a shallow estuary connecting Xiamen Bay and the Taiwan Strait, and it receives freshwater from the Jiulong River [53]. Dongshan Bay is located on the southeast coast of Fujian, China, and it is one of three excellent harbors in Fujian Province. Research on ammonium concentration in Dongshan Bay is greatly significant because it is one of the largest marine aquaculture bases in Fujian Province [54,55].

As mentioned above, an analyzing frequency of $12\,h^{-1}$ was sufficient for reaching the stable absorbance in *i*SEA. This period corresponds to a spatial resolution of ~1.2 km, assuming a cruising speed of 14 km/h. For more than 54 h, *i*SEA exhibited good stability during the 7 cruises, and the longest deployment was for 11 h on May 28, 2018. Except for special circumstances of power failure, no other maintenance was required for system operation. During the course of a cruise that was approximately 420 km, a total of 716 samples were measured, and 34 discrete samples were collected and analyzed using both *i*SEA and the classical benchtop protocol; excellent agreement was observed

Table 5
Summary of ammonium concentrations and recoveries in different aqueous samples (n = 3).

| Sample	Salinity	Added, µM	Found, µM	Added, µM	Found, µM	Recovery, %
Mineral water	0	0	ND[a]	5	4.98 ± 0.08	99.5 ± 1.6
River water 1	0	0	1.43 ± 0.13	5	6.29 ± 0.34	97.1 ± 6.7
River water 2	0	0	45.1 ± 0.46	120	158 ± 0.59	94.3 ± 0.5
Seawater 1	6	0	26.3 ± 0.30	50	77.9 ± 0.21	103 ± 0.4
Seawater 2	12	0	24.4 ± 0.48	100	123 ± 1.04	98.2 ± 1.0
Seawater 3	14	0	18.8 ± 0.23	80	99.5 ± 0.71	101 ± 0.9
Seawater 4	24	0	10.8 ± 0.10	40	54.0 ± 0.38	108 ± 1.0
Seawater 5	29	0	9.93 ± 0.14	10	20.4 ± 0.33	104 ± 3.3
Seawater 6	35	0	ND[a]	3	3.17 ± 0.08	106 ± 2.7

[a] ND, not detected.
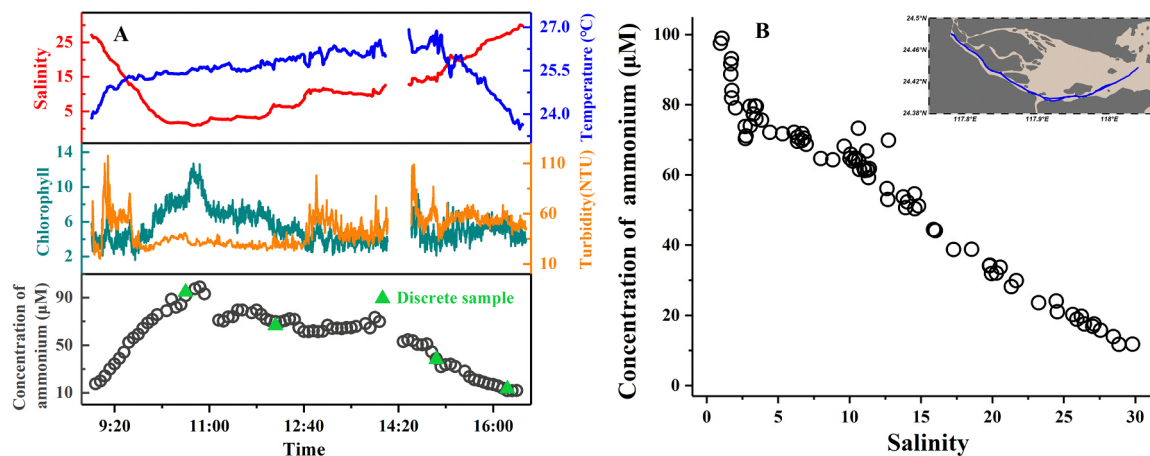
Fig. 7. Underway analysis results in Jiulongjiang Estuary. A: Ammonium concentration with temperature, salinity, chlorophyll concentration, and turbidity. (Green triangles represent the concentration of manually collected samples analyzed using the reference method.) B: Correlation of ammonium concentration with salinity. Inset: Map of route in the Jiulongjiang Estuary. (For interpretation of the references to color in this figure legend, the reader is referred to the web version of this article.)

between these two data sets (Fig. 6). Because the focus of this paper is not the nitrogen cycle, data from only 3 cruises are introduced here to demonstrate the applicability of the analyzer.

During the Jiulongjiang Estuary cruise (April 24, 2018), the research vessel *R/V Haiyang II* sailed from Xiamen Bay to Jiulongjiang Estuary, and then backtracked, as shown the inset of Fig. 7-B. Fig. 7-A illustrates the temperature, salinity, chlorophyll concentration, turbidity, and ammonium concentration values for surface water as a function of time along the transect. Overall, the turbidity of the water samples varied from 10 UNT up to approximately 110 UNT, and this indicates the efficiency of the automated filtration system for underway analysis of surface waters that contain large amounts of particles. The ammonium values range from 12 to 99 µM. This indicates an apparently negative correlation with salinity (Fig. 7-B), which is likely because the influx of seawater resulted in a lower concentration of ammonium and higher salinity. This is similar to the observations in our previous studies in which we analyzed discrete samples [9,24,42].

Using the *i*SEA system, underway surface monitoring also made a circle survey around Xiamen Island on April 23, 2018, and was conducted along a 109 km line transect from Xiamen Bay to Dongshan Bay in Taiwan Strait on May 27, 2018, during the Dongshan Swire Marine Station Sharing Cruise (DSC2018S). The distribution of surface ammonium concentrations during two cruises is presented in Fig. 8. During the underway process in the Xiamen coastal area, there was a strong spatial variation in the ammonium concentrations; concentrations ranged from 5 µM to > 40 µM. The variation may be linked to the municipal effluent near the coastal area. For ammonium concentrations during DSC2018S cruise on May 27, a maximum of 2.4 µM and a

minimum of 0.4 µM were determined; salinity varied from 31 to 34 and temperature varied from 26 to 31 °C, showing that there was lower ammonium concentration with an insignificant gradient compared with the values in Xiamen Bay.

4. Conclusions

In this study, a robust, and salinity-interference-free flow analyzer system (*i*SEA) was developed for high-frequency underway ammonium analysis in estuarine and coastal areas. The instrument meets many of the criteria for unattended field-use, such as being fully automated and being robust. It also has instrumental features that are desirable for mapping, such as fast throughput, reduced reagent consumption, and tidy sample/waste handling. It also has excellent analytical figures of sensitivity, precision, and accuracy. Compared with other flow systems, *i*SEA has the novelties of having simple hardware, having insignificant interference from salinity, and being free of the bubble problem. High-quality data obtained without any ongoing calibration for in-field application demonstrate the suitability of *i*SEA in harsh environments with steep concentration gradients and varying salinity. The automated and portable analyzer has potential application in ships of opportunity for unmanned analysis [56]. Additionally, *i*SEA has a simple configuration and can be easily modified for other spectrophotometric detection. For determination at a single wavelength, a CCD detector can be replaced with an LED/photodiode-based detection system [57,58], which is more efficient and is under development for use in more field applications.
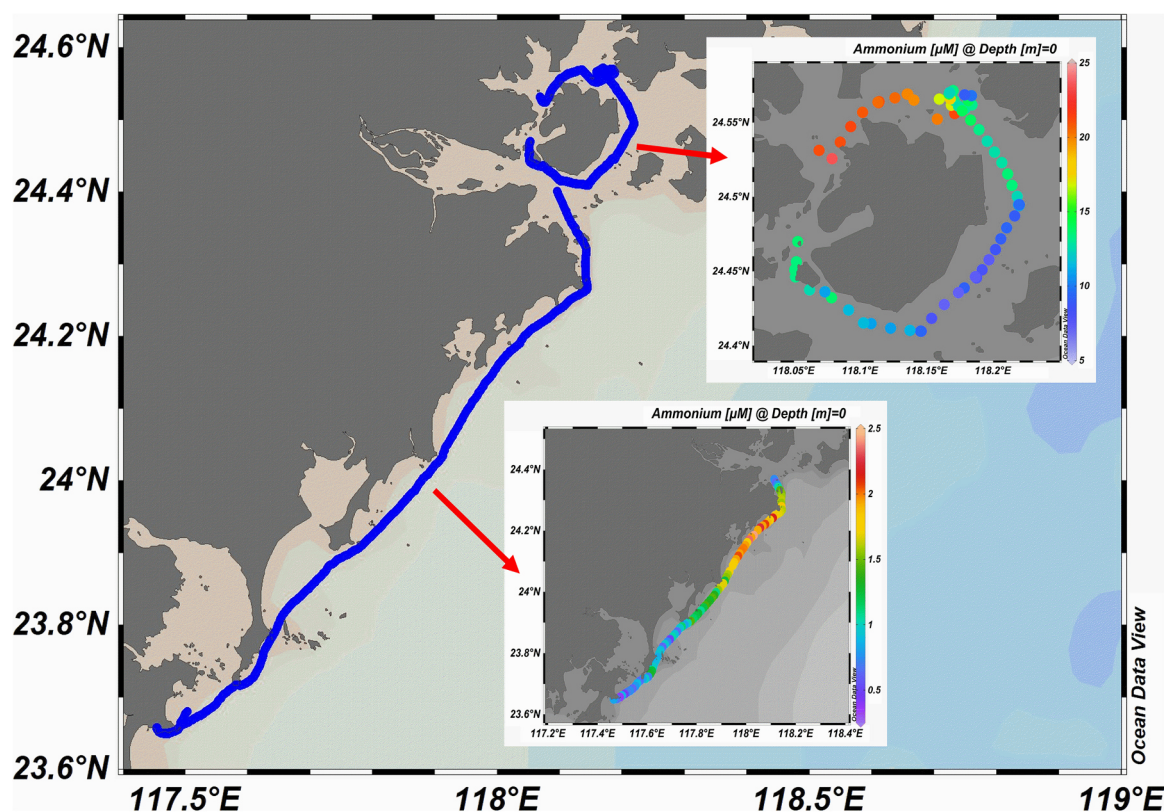
Fig. 8. Cruise track of the *R/V* Haiyang II and field observation of ammonium concentrations in Xiamen Bay cruise and DSC2018.

References

[1] J.P. Zehr, R.M. Kudela, Annu. Rev. Mar. Sci. 3 (2011) 197–225.
[2] H.W. Paerl, Mar. Chem. 206 (2018) 1–6.
[3] J.A. Brandes, A.H. Devol, C. Deutsch, Chem. Rev. 107 (2007) 577–589.
[4] L. Zhang, E.G. Xu, Y. Li, H. Liu, D.E. Vidal-Dorsch, J.P. Giesy, Chemosphere 202 (2018) 136–144.
[5] P.J. Statham, Sci. Total Environ. 434 (2012) 213–227.
[6] J.A. Camargo, Á. Alonso, Environ. Int. 32 (2006) 831–849.
[7] L.O. Šraj, M.I.G.S. Almeida, S.E. Swearer, S.D. Kolev, I.D. McKelvie, Trends Anal. Chem. 59 (2014) 83–92.
[8] A.J. Lyddy-Meaney, P.S. Ellis, P.J. Worsfold, E.C.V. Butler, I.D. McKelvie, Talanta 58 (2002) 1043–1053.
[9] N. Chen, M.D. Krom, Y. Wu, D. Yu, H. Hong, Sci. Total Environ. 628–629 (2018) 1108–1120.
[10] J. Ma, L. Adornato, R.H. Byrne, D. Yuan, Trends Anal. Chem. 60 (2014) 1–15.
[11] C. Molins-Legua, S. Meseguer-Lloret, Y. Moliner-Martinez, P. Campíns-Falcó, Trends Anal. Chem. 25 (2006) 282–290.
[12] W. Alahmad, T. Pluangklang, T. Mantim, V. Cerdà, Talanta 177 (2018) 34–40.
[13] L. Gao, X. Yang, Y. Shu, X. Chen, J. Wang, J. Colloid Interface Sci. 512 (2018) 819–825.
[14] R. Sharan, M. Roy, A.K. Tyagi, A. Dutta, Sens. Actuators B Chem. 258 (2018) 454–460.
[15] Y.B. Cho, S.H. Jeong, H. Chun, Y.S. Kim, Sens. Actuators B Chem. 256 (2018) 167–175.
[16] X. Bao, S. Liu, W. Songa, H. Gao, Anal. Methods 10 (2018) 2096–2101.
[17] A. Amirjani, D.H. Fatmehsari, Talanta 176 (2018) 242–246.
[18] L.O. Šraj, M.I.G.S. Almeidaa, C. Bassetta, I.D. McKelviea, S.D. Kolev, Talanta 181 (2018) 52–56.
[19] M. Zhang, T. Zhang, Y. Liang, Y. Pan, Sens. Actuators B Chem. 276 (2018) 356–361.
[20] C. Wang, Z. Li, Z. Pan, D. Li, Comput. Electron. Agric. 150 (2018) 364–373.
[21] G. Giakisikli, A.N. Anthemidis, Anal. Chim. Acta 1033 (2018) 73–80.
[22] Y. Zhu, J. Chen, X. Shi, D. Yuan, S. Feng, T. Zhou, Y. Huang, Anal. Methods 10 (2018) 1781–1787.
[23] T. Sukaram, P. Sirisakwisut, J. Sirirak, D. Nacapricha, S. Chaneam, Int. J. Environ. Anal.

Chem. 98 (2018) 907–920.
[24] K. Lin, P. Li, Q. Wu, S. Feng, J. Ma, D. Yuan, Microchem. J. 138 (2018) 519–525.
[25] P.J. Worsfold, R. Clough, M.C. Lohan, P. Monbet, P.S. Ellis, C.R. Quétel, G.H. Floor, I.D. Mckelvie, Anal. Chim. Acta 803 (2013) 15–40.
[26] B.S. Gentle, P.S. Ellis, P.A. Faber, M.R. Grace, I.D. McKelvie, Anal. Chim. Acta 674 (2010) 117–122.
[27] P.S. Ellis, A.M.H. Shabani, B.S. Gentle, I.D. McKelvie, Talanta 84 (2011) 98–103.
[28] R.A. Segundo, R.B.R. Mesquita, M.T.S.O.B. Ferreira, C.F.C.P. Teixeira, A.A. Bordalo, A.O.S.S. Rangel, Anal. Methods 3 (2011) 2049–2055.
[29] R.T. Masserini, K.A. Fanning, Mar. Chem. 68 (2000) 323–333.
[30] Q.P. Li, J.Z. Zhang, F.J. Millero, D.A. Hansell, Mar. Chem. 96 (2005) 73–85.
[31] C. Frank, F. Schroeder, R. Ebinghaus, W. Ruck, Microchim. Acta 154 (2006) 31–38.
[32] N. Amornthammarong, J.-Z. Zhang, Anal. Chem. 80 (2008) 1019–1026.
[33] J.N. Plant, K.S. Johnson, J.A. Needoba, L.J. Coletti, Limnol. Oceanogr. Methods 7 (2009) 144–156.
[34] S. Abi Kaed Bey, D.P. Connelly, F.E. Legiret, A.J.K. Harris, M.C. Mowlem, Ocean Dyn. 61 (2011) 1555–1565.
[35] G. Chen, M. Zhang, Z. Zhang, Y. Huang, D. Yuan, Anal. Lett. 44 (2011) 310–326.
[36] N. Amornthammarong, J.-Z. Zhang, P.B. Ortner, J. Stamates, M. Shoemaker, M.W. Kindel, Environ. Sci.: Process. Impacts 15 (2013) 579–584.
[37] Y. Zhu, D. Yuan, Y. Huang, J. Ma, S. Feng, Anal. Chim. Acta 794 (2013) 47–54.
[38] F. Hashihama, J. Kanda, A. Tauchi, T. Kodama, H. Saito, K. Furuya, Talanta 143 (2015) 374–380.
[39] R.T. Masserini Jr., K.A. Fanning, S.A. Hendrix, B.M. Kleiman, Cont. Shelf Res. 150 (2017) 48–56.
[40] J. Ma, P. Li, Z. Chen, K. Lin, N. Chen, Y. Jiang, J. Chen, B. Huang, D. Yuan, Anal. Chem. 90 (2018) 6431–6435.
[41] J. Kanda, Water Res. 29 (1995) 2746–2750.
[42] J. Ma, P. Li, K. Lin, Z. Chen, N. Chen, K. Liao, D. Yuan, Talanta 179 (2018) 608–614.
[43] Y. Zhu, D. Yuan, Y. Huang, J. Ma, S. Feng, K. Lin, Mar. Chem. 162 (2014) 114–121.
[44] N. Amornthammarong, P.B. Ortner, J.-Z. Zhang, Talanta 81 (2010) 1472–1476.
[45] R.R. Holser, M.A. Goni, B. Hales, Mar. Chem. 123 (2011) 67–77.
[46] J. Ma, Q. Li, D. Yuan, Talanta 123 (2014) 218–223.
[47] B. Liu, H. Su, S. Wang, Z. Zhang, Y. Liang, D. Yuan, J. Ma, Sens. Actuators B Chem. 237 (2016) 710–714.
[48] F.Z. Abouhiat, C. Henrıquez, B. Horstkotte, F.E. Yousfi, V. Cerdà, Talanta 108 (2013) 92–102.
[49] P.L. Searle, Analyst 109 (1984) 549–568.
[50] S.-C. Pai, Y.-J. Tsau, T.-I. Yang, Anal. Chim. Acta 434 (2001) 209–216.
[51] K. Lin, J. Pei, P. Li, J. Ma, Q. Li, D. Yuan, Talanta 185 (2018) 419–426.
[52] J.-Z. Zhang, J. Autom. Chem. 19 (1997) 205–212.
[53] N. Chen, Q. Mo, Y. Kuo, Y. Su, Y. Zhong, Sci. Total Environ. 619–620 (2018) 301–310.
[54] Z. Wang, Environ. Prot. Sci. 41 (2015) 93–97 (in Chinese with English abstract).
[55] S. Jiang, P. Lin, L. Wu, H. Zheng, J. Cai, Y. Xi, S. Zheng, M. Yang, S. Zhong, Mar. Dev. Manag. 12 (2016) 39–48 (in Chinese with English abstract).
[56] G.R.D. Prabhu, P.L. Urban, Trends Anal. Chem. 88 (2017) 41–52.
[57] D.A. Bui, P.C. Hauser, Anal. Chim. Acta 853 (2015) 46–58.
[58] M. Macka, T. Piasecki, P.K. Dasgupta, Annu. Rev. Anal. Chem. 7 (2014) 2.1–2.25.